npj | 2D Materials and Applications

www.nature.com/npj2dmaterials

ARTICLE OPEN

Room-temperature magnetism and tunable energy gaps in edge-passivated zigzag graphene quantum dots

Wei Hu[1,2], Yi Huang[3,4,5], Xinmin Qin[1], Lin Lin[2,4], Erjun Kan[6], Xingxing Li[1], Chao Yang[2] and Jinlong Yang[1]

Graphene is a nonmagnetic semimetal and cannot be directly used as electronic and spintronic devices. Here, we demonstrate that zigzag graphene nanoflakes (GNFs), also known as graphene quantum dots, can exhibit strong edge magnetism and tunable energy gaps due to the presence of localized edge states. By using large-scale first principle density functional theory calculations and detailed analysis based on model Hamiltonians, we can show that the zigzag edge states in GNFs ($C_{6n^2}H_{6n}$, $n = 1$–25) become much stronger and more localized as the system size increases. The enhanced edge states induce strong electron–electron interactions along the edges of GNFs, ultimately resulting in a magnetic configuration transition from nonmagnetic to intra-edge ferromagnetic and inter-edge antiferromagnetic, when the diameter is larger than 4.5 nm ($C_{480}H_{60}$). Our analysis shows that the inter-edge superexchange interaction of antiferromagnetic states between two nearest-neighbor zigzag edges in GNFs at the nanoscale (around 10 nm) can be stabilized at room temperature and is much stronger than that exists between two parallel zigzag edges in graphene nanoribbons, which cannot be stabilized at ultra-low temperature (3 K). Furthermore, such strong and localized edge states also induce GNFs semiconducting with tunable energy gaps, mainly controlled by adjusting the system size. Our results show that the quantum confinement effect, inter-edge superexchange (antiferromagnetic), and intra-edge direct exchange (ferromagnetic) interactions are crucial for the electronic and magnetic properties of zigzag GNFs at the nanoscale.

npj 2D Materials and Applications (2019)3:17 ; https://doi.org/10.1038/s41699-019-0098-2

INTRODUCTION

Engineering techniques that use finite size effect to introduce tunable edge magnetism and energy gap are by far the most promising ways for enabling graphene[1] to be used in electronics and spintronics.[2,3] Examples of finize-sized graphene nanostructures include one-dimensional (1D) graphene nanoribbons (GNRs)[4–16] and zero-dimensional (0D) graphene nanoflakes (GNFs) (also known as graphene quantum dots).[17–28] It is well known that electronic and magnetic properties[29] of GNRs and GNFs depend strongly on the atomic configuration of their edges, which are of either the armchair (AC) or zigzag (ZZ) types.[8]

Edge magnetism has been predicted theoretically[10,11] and observed experimentally[15,16] in ZZGNRs. The magnetism in ZZGNRs results from ferromagnetic (FM) coupling for each zigzag edge and antiferromagnetic (AFM) coupling between two parallel zigzag edges of ZZGNRs. The strong FM coupling along each zigzag edge has been predicted in theory[11] and confirmed in experiments.[16] However, the AFM coupling between two parallel zigzag edges in ZZGNRs is weak, which cannot be stabilized even at low temperature below 10 K[14] and rapidly weakens ($\sim w^{-2}$) as the ribbon-width w increases.[13] Furthermore, the energy gap of GNRs depend on several factors, such as the edge type (armchair or zigzag) and the width of the nanoribbon,[8] thus cannot be easily tuned. Such problem does not exist in GNFs due to the quantum confinement effect.[30] The ability to control the energy gap has enabled GNFs to be used in promising applications in electronics.[20] In addition, triangular ZZGNFs are theoretically predicted to have strong edge magnetism even in small systems.[31,32] However, triangular ZZGNFs have large formation energy[24] and have not been synthesized experimentally. Fortunately, hexagonal ZZGNFs exhibits significantly improved stability in ambient environment.[24] Recent experiments[33] have also demonstrated that edge magnetism can be observed in ZZGNFs when the edges are passivated by certain chemical groups. However, semi-empirical tight-binding model[34,35] and first principle density functional theory (DFT) calculations[25–28] for hexagonal ZZGNFs have been performed for small-sized systems but found no magnetism (NM). Thus the prospect of finding stable finite-sized graphene easily fabricated in experiments with both strong edge magnetism and tunable energy gap seems dim.

In this letter, we systematically investigate the electronic and magnetic properties of hexagonal ZZGNFs with the diameters in the range of 1–12 nm (from $C_{24}H_{12}$ to $C_{3750}H_{150}$). Using first-principles DFT calculations, we find that both strong edge magnetism and tunable energy gap can be realized simultaneously in large ZZGNFs stabilized at room temperature. We demonstrate that spin polarization plays a crucial role as the diameter of a ZZGNF increases beyond 4.5 nm ($C_{486}H_{54}$). A spin-unpolarized calculation shows that edge states become increasingly more localized as the size of a ZZGNF increases. These edge states form a half-filled pseudo-band and is thus unstable. Adding spin-polarization allows the edge states to spontaneously split into

[1]Hefei National Laboratory for Physical Sciences at Microscale, Department of Chemical Physics, and Synergetic Innovation Center of Quantum Information and Quantum Physics, University of Science and Technology of China, 230026 Hefei, Anhui, China; [2]Computational Research Division, Lawrence Berkeley National Laboratory, Berkeley, CA 94720, USA; [3]Department of Applied Physics, Xi'an Jiaotong University, 710049 Xi'an, Shaanxi, China; [4]Department of Mathematics, University of California, Berkeley, CA 94720, USA; [5]School of Physics and Astronomy, University of Minnesota, Minneapolis, MN 55455, USA and [6]Department of Applied Physics and Institution of Energy and Microstructure, Nanjing University of Science and Technology, 210094 Nanjing, Jiangsu, China
Correspondence: Lin Lin (linlin@math.berkeley.edu) or Chao Yang (cyang@lbl.gov) or Jinlong Yang (jlyang@ustc.edu.cn)

Received: 8 October 2018 Accepted: 18 March 2019
Published online: 16 April 2019

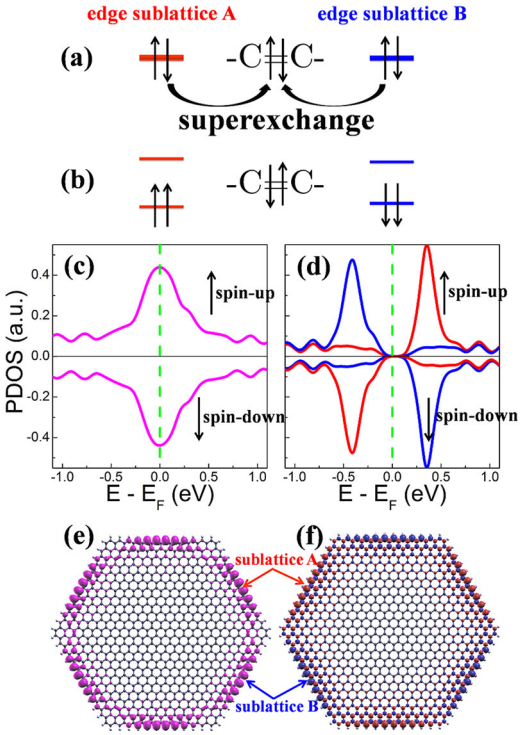

Fig. 1 **a** Relative energy per edge atom (ΔE(AFM-NM) and ΔE(AFM-FM)) of NM, AFM, and FM coupling between different edges in ZZGNFs and ZZGNRs and (**b**) spin electron density $<\hat{n}_{i\sigma}gt;$ ($\sigma = \uparrow$ (spin-up) or $\downarrow$ (spin-down)) at the carbon atom i in the middle of each zigzag edge in AFM ZZGNFs under the variation of the diameter size (ZZGNFs) or ribbon-width length size (ZZGNRs). The red and blue regions represent the stable NM (ΔE(AFM–NM) ≈ 0) and AFM (ΔE(AFM–NM) < 0) coupling between different edges in ZZGNFs, respectively. The critical temperature is estimated by the mean-field theory $T = \Delta E/k_B$, where k_B is the Boltzmann constant

spin-polarized occupied and unoccupied states. This separation results in a magnetic configuration transition from an NM configuration to a strong inter-edge AFM configuration. It also opens a tunable band gap that can be easily controlled by quantum confinement effect. These properties make GNFs better candidate materials for nanoelectronics than GNRs.[8] We also confirm that ZZGNFs passivated by different chemical groups all exhibit similar behavior. Such flexibility may facilitate future experimental synthesis of such ZZGNFs.

RESULTS AND DISCUSSION

We demonstrate the importance of spin polarization using $C_{864}H_{72}$ (6 nm) as an example (Fig. 2). From a spin-unpolarized calculation, we observe strong and localized edge states (Fig. 2e). These edge states contribute to high electron density along the edges of $C_{864}H_{72}$. Furthermore, these edge states become much stronger and more localized as the ZZGNF size increases.[28] The presence of strong edge states makes the ZZGNF metallic at the nanoscale.[35] The projected density of states (PDOS) of carbon edges of $C_{864}H_{72}$ plotted in Fig. 2c clearly show a considerably high density of states (DOS) near the Fermi level. This figure confirms that $C_{864}H_{72}$ is predicted to be metallic in a spin-unpolarized calculation. The metallic nature of the ZZGNF can be attributed to the presence of strong localized edge states.[28]

However, a spin-polarized calculation shows that half-filled metallic edge states are not stable, and can spontaneously split into two types of occupied and unoccupied states as shown in Fig. 2b, d. As a result, a magnetic configuration transition from a non-magnetic (NM) configuration to a magnetic configuration that exhibits intra-edge FM and inter-edge AFM characters can be observed in Fig. 2f. This transition can be interpreted as the consequence of Mott-type competition between the kinetic (hopping) energy and the intra-edge (on-site) electron–electron interaction energy as the system size increases. Lowering kinetic energy by increasing the system size tends to produce delocalized spin states across all edges, while reducing the electron–electron interaction energy as the system size tends to penalize simultaneous occupation of the same edge by spin up and spin down electrons. Both semi-local GGA-PBE and hybrid HSE06 calculations (the details are given in the Supplemental Material) indicate that for small systems, kinetic energy plays a more dominant role. This observation agrees with previous theoretical prediction of the NM configuration for hexagonal ZZGNFs.[25–28,34,35] Only as the system size increases, the effective electron–electron interaction energy associated with the edge states starts to dominate and is ultimately responsible for this magnetic configuration transition.

Figure 1a shows the variation of relative energy of NM, AFM, and FM magnetic configurations in ZZGNFs and ZZGNRs, respectively, with respect to system size. Our calculations show that AFM states are much more stable than NM and FM states in large ZZGNFs, and a magnetic configuration transition occurs as the diameter of the ZZGNF becomes larger than 4.5 nm ($C_{486}H_{54}$).[31] We believe the FM coupling along each zigzag edge that belong to the same sublattice, are likely to be induced by intra-edge direct exchange interactions. The AFM coupling between two nearest-neighbor edges belonging to different sublattices are likely to be induced by inter-edge superexchange interactions facilitated by a carbon–carbon double bond (C=C) at the corner where two nearest-neighbor edges meet in ZZGNFs at the nanoscale. The local magnetic moment defined by $M_i = |<\hat{n}_{i\uparrow}gt; - <\hat{n}_{i\downarrow}>|$, where $<\hat{n}_{i\sigma}gt;$ is spin electron density with $\sigma = \uparrow$ (spin-up) or $\downarrow$ (spin-down)), at the carbon atom i. Figure 2b shows the local magnetic moment of carbon in the the middle of each zigzag edge in ZZGNFs (with the largest magnetic moment) increases with the system size, and converges to $0.3\mu_B$ when the diameter is larger than than 6 nm ($C_{864}H_{72}$). Furthermore, there is no charge transfer ($<\hat{n}_{i\uparrow}gt; + <\hat{n}_{i\downarrow}gt; \approx 4$) between carbon atoms

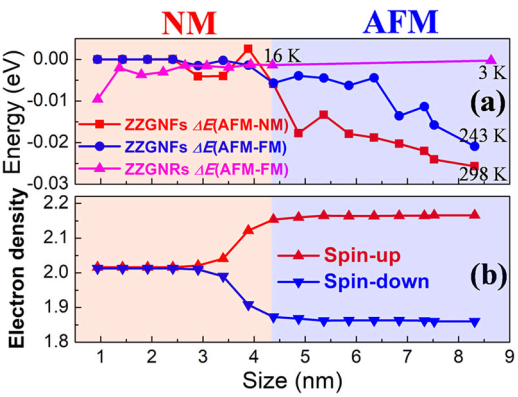

Fig. 2 Electronic structure of edge states in $C_{864}H_{72}$ in two different magnetic configurations (NM and AFM), including the schematic illustration of orbital diagram of superexchange interaction of edge states in the (**a**) NM and (**b**) AFM configurations, projected density of states (PDOS) of edges in the (**c**) NM and (**d**) AFM configurations, (**e**) local density of states (LDOS) of Fermi level (pink isosurfaces) in the NM configuration and (**f**) spin density isosurfaces in the AFM configuration. The red and blue isosuraces in (**f**) represent the spin-up and spin-down states, respectively. The red and blue lines in (**d**) represent the PDOS contributed by sublattice A (spin-up edges) and B (spin-down edges) atoms in graphene, respectively. The fermi level is marked by green dotted lines and set to zero

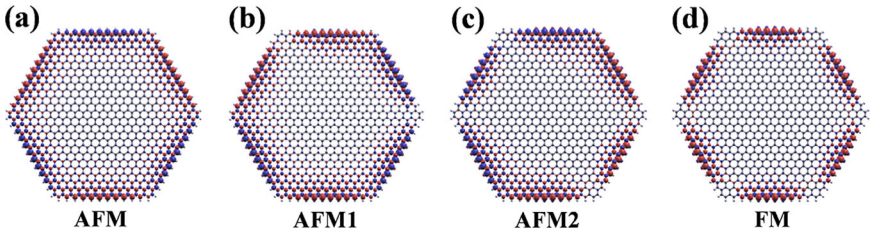

Fig. 3 Spin density isosurfaces of hydrogen-passivated $C_{864}H_{72}$ in four different magnetic states, three types of antiferromagnetic ((**a**) AFM, (**b**) AFM1, and (**c**) AFM2) and one type of ferromagnetic ((**d**) FM) coupling at the inter edges. The red and blue isosurfaces represent the spin-up and spin-down states, respectively

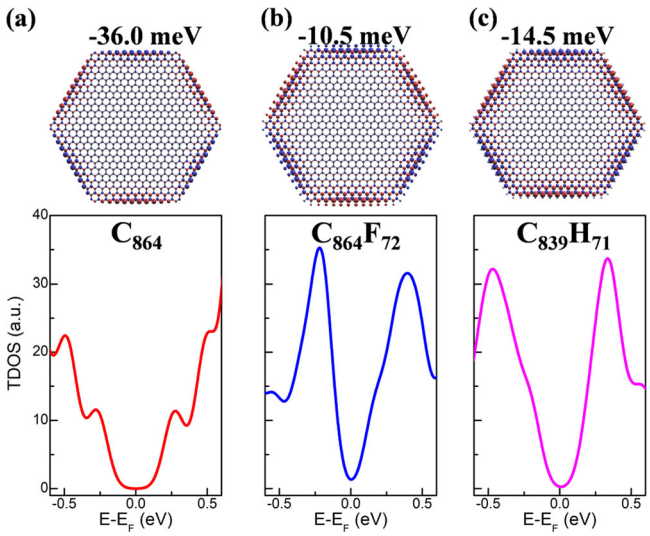

Fig. 4 Spin density isosurfaces and total density of states (TDOS) of (**a**) bare (C_{864}), (**b**) fluorine-passivated ($C_{864}F_{72}$), and (**c**) non-hexagonal ($C_{839}H_{71}$) ZZGNFs in the AFM configuration. The red and blue isosurfaces represent the spin-up and spin-down states, respectively. The energy differences ($E_{AFM}-E_{NM}$) between AFM and NM configurations of these ZZGNFs are shown above the figures. For hexagonal hydrogen-passivated $C_{864}H_{72}$, $\Delta E(\mathrm{AFM}-\mathrm{NM}) = -17.9$ meV. The fermi level is marked by green dotted lines and set to zero

sitting on different edges that belong to the same or different sublattices in ZZGNFs as the system size increases.

Notice that the intra-edge direct exchange interaction via FM coupling along each zigzag edge in ZZGNFs is similar to that in ZZGNRs. However, the inter-edge superexchange interaction via AFM coupling between two nearest-neighbor edges through a C=C bond (Fig. 2a) in ZZGNFs can be stabilized at room temperature (298 K) and is much stronger than that via AFM coupling between two parallel edges though π-bonds in ZZGNRs as shown in Fig. 1a, where such AFM spin polarization weakens rapidly as the ribbon-width increases in ZZGNRs[13] and cannot be stabilized even at ultra-low temperature (3 K).[14] Our DFT calculations confirm that the energy difference associated with AFM and FM coupling between two parallel edges in large-scale 1D ZZGNRs is negligible compared to that reported in ZZGNFs.

The enhanced stability of spin-polarized ZZGNFs can be understood by using the Heisenberg model. We consider each FM edge as one site and enumerate all possible magnetic configurations, and the Hamiltonian can be written as

$$\hat{H} = -\sum J_{i,j}\overrightarrow{M_i}\overrightarrow{M_j} \tag{1}$$

where $J_{i,j}$ is the exchange parameter between two sites i and j, $\overrightarrow{M_i}$ and $\overrightarrow{M_j}$ are the corresponding spin magnetic moments. There are four different magnetic states in $C_{864}H_{72}$, there of which are AFM, AFM1, and AFM2 configurations and one is FM configuration as shown in Fig. 3. The total energies of magnetic configurations E (AFM), E(AFM1), E(AFM2), and E(FM) can be computed by DFT calculations, and the exchange parameters can be evaluated by solving the following least-squares-fitting problem[36]

$$\begin{aligned} E(\mathrm{AFM}) &= (6J_1 - 6J_2 + 3J_3)M^2 + E_0 \\ E(\mathrm{AFM1}) &= (2J_1 + 2J_2 - J_3)M^2 + E_0 \\ E(\mathrm{AFM2}) &= (-J_1 + 2J_2 + 3J_3)M^2 + E_0 \\ E(\mathrm{FM}) &= (-6J_1 - 6J_2 - 3J_3)M^2 + E_0 \end{aligned} \tag{2}$$

where J_1, J_2, and J_3 are ortho-edge, meta-edge, and para-edge exchange interaction parameters, respectively, M is the spin magnetic moment at each edge, and E_0 is the nonmagnetic reference total energy. The solution yields $J_1 = -0.038351$ eV, $J_2 = 0.000954$ eV, and $J_3 = 0.001633$ eV for two nearest-neighbor edges of $C_{864}H_{72}$, which are 10 times stronger than the exchange interaction parameters between two parallel edges in ZZGNFs and ZZGNRs. Therefore, ZZGNFs at the nanoscale have strong edge magnetism at room temperature and can be directly used in nanospintronics, superior to that in ZZGNRs at the nanoscale.[7,13]

We perform ab initio molecular dynamics (AIMD) simulations on ZZGNFs and check the effect of temperature on electronic and magnetic properties of $C_{486}H_{54}$ in different AFM and FM configurations (the details are given in the Supplemental Material). We find that the AFM configuration of $C_{486}H_{54}$ can remain stable at room temperature of $T = 300$ K at least within 1.6 ps. Furthermore, the FM configuration of $C_{486}H_{54}$ rapidly transfers into the AFM configuration within 30.0 fs at room temperature of $T = 300$ K. Furthermore, after $t = 1.5$ ps, $C_{486}H_{54}$ is slightly bent,[26] although it still keeps the AFM configuration.

We also check the effects of using different types of atoms (e.g., bare and fluorine) to passivate ZZGNFs, and how the shape (non-hexagonal) of ZZGNFs may alter their electronic and magnetic properties. We find that magnetic configuration transition (from NM to AFM) and semiconductor characteristics (The energy gaps of 0.54, 0.34, and 0.41 eV, respectively, for bare C_{864}, fluorine-passivated $C_{864}F_{72}$ and non-hexagonal $C_{839}H_{71}$) of ZZGNFs are independent of the type of passivating atoms[37] as plotted in Fig. 4. These properties suggest that it is relatively easy to create a chemical environment in which the synthesis of large scales ZZGNFs with tunable edge magnetism and energy gaps can be easily accommodated. The possibility of rapid synthesis makes ZZGNFs ideal candidates for electronic and spintronic devices.[38]

We remark that magnetic configuration transition and the associated tunable electronic structures in ZZGNFs, especially energy gaps, can also be understood in terms of the Hubbard model.[31] From our first principle calculations, we find that choosing the parameters $t = 2.5$ eV and $U = 2.1$ eV in the Hubbard model can well reproduce the size-dependent energy gaps (the details are given in the Supplemental Material). In Fig. 5, we plot how the HOMO-LUMO energy gap E_g changes with respect to the size of ZZGNFs and ACGNFs in two different magnetic configurations (NM and AFM). Our DFT calculations and mean-field Hubbard

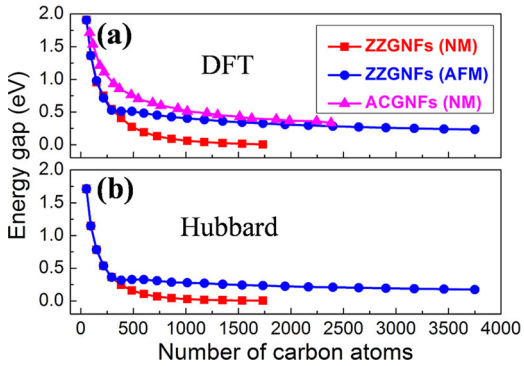

Fig. 5 Energy gap E_g (eV) of ZZGNFs and ACGNFs in two different magnetic configurations (NM and AFM) as a function of the number of carbon atoms, computed with two different methods: (**a**) DFT calculations and (**b**) Hubbard model ($t = 2.5$ eV and $U = 2.1$ eV)

model show similar results, i.e., the energy gap E_g of ZZGNF decreases as its size increases. In particular, we find that the energy gap of NM ZZGNFs decreases more rapidly with respect to the system size than that of AFM ZZGNFs, due to the presence of edge states whose electron density near the edges of ZZGNFs as shown in Fig. 2e. This observation is consistent with previous results obtained from tight-binding models[34,35] and DFT calculations.[27,28] However, AFM semiconducting ZZGNFs show similar energy gap scaling compared to that of NM ACGNFs at the nanoscale.[28] Therefore, edge states should have little effect on the energy gaps of AFM ZZGNFs and the quantum confinement effect[30] is the only factor to control the energy gaps in ZZGNFs and ACGNFs (Fig. 5a). In detail, NM ZZGNFs exhibits metallic characters (E_g is smaller than the thermal fluctuation (25 meV) at room temperature) when the diameter is larger than 7 nm ($C_{1350}H_{90}$), but AFM ZZGNFs with the diameter of 12 nm ($C_{3750}H_{150}$) still behaves as a semiconductor with a sizable energy gap $E_g = 0.23$ eV, similar to the case of NM ACGNFs.[28] Therefore, ZZGNFs at the nanoscale can be directly used in nanoelectronics.

In summary, using large-scale first principle calculations, we demonstrate that the electronic and magnetic properties of hexagonal zigzag that graphene nanoflakes (ZZGNFs) can be significantly affected by the system size. We found that the zigzag edge states in ZZGNFs become much stronger and more localized as the system size increases. The presence of these edge states induce strong electron–electron interactions along the edges of ZZGNFs, resulting in a magnetic configuration transition from nonmagnetic to intra-edge FM and inter-edge AFM when the diameter is larger than 4.5 nm. On the other hand, such strong and localized edge states are also responsible for making ZZGNFs semiconducting with a tunable energy gap. The energy gap can be controlled by merely adjusting the system size. Therefore, ZZGNFs with strong edge magnetism, tunable energy gaps and room-temperature stability may be promising candidates for practical electronic and spintronic applications.

METHODS

We use the Kohn–Sham DFT-based electronic structure analysis tools implemented in the Spanish Initiative for Electronic Simulations with Thousands of Atoms (SIESTA)[39] software package. We use the generalized gradient approximation of Perdew, Burke, and Ernzerhof (GGA–PBE)[40] exchange correlation functional with collinear spin polarization, and the double zeta plus polarization orbital basis set (DZP) to describe the valence electrons within the framework of a linear combination of numerical atomic orbitals (LCAO).[41] Because semi-local GGA–PBE calculations are less reliable in predicting the electronic structures of ZZGNFs, the screened hybrid HSE06[42] calculations implemented in HONPAS[43–45] (Hefei Order-N Packages for Ab Initio Simulations based on SIESTA) are also used to compute the electronic and magnetic properties of ZZGNFs. All atomic coordinates are fully relaxed using the conjugate gradient (CG) algorithm until the energy and force convergence criteria of 10^{-4} eV and 0.02 eV/Å, respectively, are reached.

For initial magnetic moment setting of spin-polarized DFT calculations in ZZGNFs, we set all the carbon atoms with initial magnetic moments of $1\mu_B$ for the FM configuration and only set the edged carbon atoms with initial magnetic moments of 1 or $-1\mu_B$, and then optimize the structures and magnetic moments of ZZGNFs.

Due to the large number of atoms contained in hexagonal hydrogen-passivated ZZGNFs ($C_{6n^2}H_{6n}$, $n = 1$–25), we use the recently developed Pole EXpansion and Selected Inversion (PEXSI) method[46–48] to accelerate the eigenvalue problem in the Kohn–Sham DFT calculations. The PEXSI technique can efficiently utilize the sparsity of the Hamiltonian and overlap matrices generated in SIESTA and overcome the cubic scaling limit for solving Kohn–Sham DFT, and scales at most as quadratic scaling even for metallic systems, such as graphene. Furthermore, the PEXSI method is highly scalable[49] and can scale up to 100,000 processors on high performance machines.

We perform AIMD simulations on ZZGNFs to check the effect of temperature on electronic and magnetic properties of ZZGNFs. The simulations are performed for about 1.6 ps with a time step of 2.0 fs at room temperature of $T = 300$ K controlled by a Nose–Hoover thermostat.[50,51]

DATA AVAILABILITY

The authors confirm that the data supporting the findings of this study are available within the article and its Supplementary Materials.

ACKNOWLEDGEMENTS

This work was performed, in part, under the auspices of the U.S. Department of Energy by Lawrence Livermore National Laboratory under Contract DE-AC52-07NA27344. Support for this work was provided through Scientific Discovery through Advanced Computing (SciDAC) program funded by U.S. Department of Energy, Office of Science, Advanced Scientific Computing Research and Basic Energy Sciences (W.H., L.L., and C.Y.), by the Center for Applied Mathematics for Energy Research Applications (CAMERA), which is a partnership between Basic Energy Sciences and Advanced Scientific Computing Research at the U.S. Department of Energy (L.L. and C.Y.), and by the Department of Energy under Grant No. DE-SC0017867 (L.L.). This work is also partially supported by the National Key Research and Development Program of China (Grant no. 2016YFA0200604) and the National Natural Science Foundation of China (NSFC) (Grant nos. 21688102, 51522206, and 21803066), and the Strategic Priority Research Program of Chinese Academy of Sciences (Grant no. XDC01000000), the Research Start-Up Grants (Grant no. KY2340000094) from University of Science and Technology of China, and the Chinese Academy of Sciences Pioneer Hundred Talents Program. Y.H. acknowledges support from the Education Program for Talented Students of Xi'an Jiaotong University. We thank the National Energy Research Scientific Computing (NERSC) center, and the USTCSCC, SC-CAS, Tianjin, and Shanghai Supercomputer Centers for the computational resources.

AUTHOR CONTRIBUTIONS

W.H., L.L., E.K., C.Y., and J.Y. designed the idea of this manuscript and supported this project. W.H. performed all the DFT calculations in SIESTA. Y.H. wrote the codes of Hubbard model. X.Q. performed the hybrid HSE06 calculations in HONPAS. All the authors helped to write, modify, and analyze this manuscript.

ADDITIONAL INFORMATION

Supplementary Information accompanies the paper on the *npj 2D Materials and Applications* website (https://doi.org/10.1038/s41699-019-0098-2).

Competing interests: The authors declare no competing interests.

Publisher's note: Springer Nature remains neutral with regard to jurisdictional claims in published maps and institutional affiliations.

REFERENCES

1. Novoselov, K. S. et al. Electric field effect in atomically thin carbon films. *Science* **306**, 666–669 (2004).
2. Geim, A. K. & Novoselov, K. S. The rise of graphene. *Nat. Mater.* **6**, 183–191 (2007).

3. Neto, A. H. C., Guinea, F., Peres, N. M. R., Novoselov, K. S. & Geim, A. K. The electronic properties of graphene. *Rev. Mod. Phys.* **18**, 109 (2009).
4. Han, M. Y., Özyilmaz, B., Zhang, Y. & Kim, P. Energy band-gap engineering of graphene nanoribbons. *Phys. Rev. Lett.* **98**, 206805 (2007).
5. Li, X., Wang, X., Zhang, L., Lee, S. & Dai, H. Chemically derived, ultrasmooth graphene nanoribbon semiconductors. *Science* **319**, 1229–1232 (2008).
6. Jia, X. et al. Controlled formation of sharp zigzag and armchair edges in graphitic nanoribbons. *Science* **323**, 1701–1705 (2009).
7. Son, Y.-W., Cohen, M. L. & Louie, S. G. Half-metallic graphene nanoribbons. *Nature* **444**, 347–349 (2006).
8. Son, Y.-W., Cohen, M. L. & Louie, S. G. Energy gaps in graphene nanoribbons. *Phys. Rev. Lett.* **97**, 216803 (2006).
9. Yang, L., Park, C.-H., Son, Y.-W., Cohen, M. L. & Louie, S. G. Quasiparticle energies and band gaps in graphene nanoribbons. *Phys. Rev. Lett.* **99**, 186801 (2007).
10. Kan, E., Li, Z., Yang, J. & Hou, J. G. Half-metallicity in edge-modified zigzag graphene nanoribbons. *J. Am. Chem. Soc.* **130**, 4224–4225 (2008).
11. Yazyev, O. V. & Katsnelson, M. I. Magnetic correlations at graphene edges: Basis for novel spintronics devices. *Phys. Rev. Lett.* **100**, 047209 (2008).
12. Long, M.-Q., Tang, L., Wang, D., Wang, L. & Shuai, Z. Theoretical predictions of size-dependent carrier mobility and polarity in graphene. *J. Am. Chem. Soc.* **131**, 17728–17729 (2009).
13. Jung, J., Pereg-Barnea, T. & MacDonald, A. H. Theory of interedge superexchange in zigzag edge magnetism. *Phys. Rev. Lett.* **102**, 227205 (2009).
14. Kunstmann, J., Özdoğan, C., Quandt, A. & Fehske, H. Stability of edge states and edge magnetism in graphene nanoribbons. *Phys. Rev. B* **83**, 045414 (2011).
15. Magda, G. Z. et al. Room-temperature magnetic order on zigzag edges of narrow graphene nanoribbons. *Nature* **514**, 608–611 (2014).
16. Ruffieux, P. et al. On-surface synthesis of graphene nanoribbons with zigzag edge topology. *Nature* **531**, 489–492 (2016).
17. Ponomarenko, L. A. et al. Chaotic dirac billiard in graphene quantum dots. *Science* **320**, 356–358 (2008).
18. Shang, N. G. et al. Catalyst-free efficient growth, orientation and biosensing properties of multilayer graphene nanoflake films with sharp edge planes. *Adv. Funct. Mater.* **18**, 3506–3514 (2008).
19. de Parga, A. L. V. et al. Periodically rippled graphene: Growth and spatially resolved electronic structure. *Phys. Rev. Lett.* **100**, 056807 (2008).
20. Ritter, K. A. & Lyding, J. W. The influence of edge structure on the electronic properties of graphene quantum dots and nanoribbons. *Nat. Mater.* **8**, 235–242 (2009).
21. Kuc, A., Heine, T. & Seifert, G. Structural and electronic properties of graphene nanoflakes. *Phys. Rev. B* **81**, 085430 (2010).
22. Wimmer, M., Akhmerov, A. R. & Guinea, F. Robustness of edge states in graphene quantum dots. *Phys. Rev. B* **82**, 045409 (2010).
23. Eda, G. et al. Blue photoluminescence from chemically derived graphene oxide. *Adv. Mater.* **22**, 505–509 (2010).
24. Lin, P.-C. et al. Nano-sized graphene flakes: Insights from experimental synthesis and first principles calculations. *Phys. Chem. Chem. Phys.* **19**, 6338–6344 (2017).
25. Zhou, Y. et al. Hydrogenated graphene nanoflakes: semiconductor to half-metal transition and remarkable large magnetism. *J. Phys. Chem. C* **116**, 5531–5537 (2012).
26. Wohner, N., Lam, P. & Sattler, K. Energetic stability of graphene nanoflakes and nanocones. *Carbon* **67**, 721 (2014).
27. Singh, S. K., Neek-Amal, M. & Peeters, F. M. Electronic properties of graphene nano-flakes: energy gap, permanent dipole, termination effect, and raman spectroscopy. *J. Chem. Phys.* **140**, 074304 (2014).
28. Hu, W., Lin, L., Yang, C. & Yang, J. Electronic structure and aromaticity of large-scale hexagonal graphene nanoflakes. *J. Chem. Phys.* **141**, 214704 (2014).
29. Yazyev, O. V. Emergence of magnetism in graphene materials and nanostructures. *Rep. Prog. Phys.* **73**, 056501 (2010).
30. Raty, J., Galli, G. & van Buuren, T. Quantum confinement and fullerenelike surface reconstructions in nanodiamonds. *Phys. Rev. Lett.* **90**, 037401 (2003).
31. Fernández-Rossier, J. & Palacios, J. J. Magnetism in graphene nanoislands. *Phys. Rev. Lett.* **99**, 177204 (2007).
32. Wang, W. L., Meng, S. & Kaxiras, E. Graphene nanoflakes with large spin. *Nano Lett.* **8**, 241–245 (2008).
33. Sun, Y. et al. Magnetism of graphene quantum dots. *npj Quantum Mater.* **2**, 5 (2017).
34. Zhang, Z. Z., Chang, K. & Peeters, F. M. Tuning of energy levels and optical properties of graphene quantum dots. *Phys. Rev. B* **77**, 235411 (2008).
35. Güçlü, A. D., Potasz, P. & Hawrylak, P. Excitonic absorption in gate-controlled graphene quantum dots. *Phys. Rev. B* **82**, 155445 (2010).
36. Li, X., Wu, X. & Yang, J. Room-temperature half-metallicity in la(mn,zn)aso alloy via element substitutions. *J. Am. Chem. Soc.* **136**, 5664–5669 (2014).
37. Kabir, M. & Saha-Dasgupta, T. Manipulation of edge magnetism in hexagonal graphene nanoflakes. *Phys. Rev. B* **90**, 035403 (2014).
38. Hawrylak, P., Peeters, F. & Ensslin, K. Carbononics—integrating electronics, photonics and spintronics with graphene quantum dots. *Phys. Status Solidi RRL* **10**, 11–12 (2016).
39. Soler, J. M. et al. The siesta method for ab initio order-n materials simulation. *J. Phys.: Condens. Matter* **14**, 2745 (2002).
40. Perdew, J. P., Burke, K. & Ernzerhof, M. Generalized gradient approximation made simple. *Phys. Rev. Lett.* **77**, 3865 (1996).
41. Junquera, J., Paz, O., Sánchez-Portal, D. & Artacho, E. Numerical atomic orbitals for linear-scaling calculations. *Phys. Rev. B* **64**, 235111 (1996).
42. Heyd, J., Scuseria, G. E. & Ernzerhof, M. Erratum: "hybrid functionals based on a screened coulomb potential" [J. Chem. Phys. 118, 8207 (2003)]. *J. Chem. Phys.* **124**, 219906 (2006).
43. Shang, H., Li, Z. & Yang, J. Implementation of exact exchange with numerical atomic orbitals. *J. Phys. Chem. A* **114**, 1039–1043 (2010).
44. Shang, H., Li, Z. & Yang, J. Implementation of screened hybrid density functional for periodic systems with numerical atomic orbitals: basis function fitting and integral screening. *J. Chem. Phys.* **135**, 034110 (2011).
45. Qin, X., Shang, H., Xiang, H., Li, Z. & Yang, J. Honpas: a linear scaling open-source solution for large system simulations. *Int. J. Quantum Chem.* **115**, 647–655 (2014).
46. Lin, L., Lu, J., Ying, L., Car, R. & E, W. Fast algorithm for extracting the diagonal of the inverse matrix with application to the electronic structure analysis of metallic systems. *Commun. Math. Sci.* **7**, 755–777 (2009).
47. Lin, L., Chen, M., Yang, C. & He, L. Accelerating atomic orbital-based electronic structure calculation via pole expansion and selected inversion. *J. Phys.: Condens. Matter* **25**, 295501 (2013).
48. Lin, L., Garca, A., Huhs, G. & Yang, C. SIESTA-PEXSI: massively parallel method for efficient and accurate ab initio materials simulation without matrix diagonalization. *J. Phys.: Condens. Matter* **26**, 305503 (2014).
49. Hu, W., Lin, L. & Yang, C. DGDFT: a massively parallel method for large scale density functional theory calculations. *J. Chem. Phys.* **143**, 124110 (2015).
50. Nosé, S. A unified formulation of the constant temperature molecular dynamics methods. *J. Chem. Phys.* **81**, 511 (1984).
51. Hoover, W. G. Canonical dynamics: equilibrium phase-space distributions. *Phys. Rev. A* **31**, 1695 (1985).